Electron-ion collider transverse instabilities due to the crab cavity fundamental impedance

T. Mastoridis and T. Loe
California Polytechnic State University, San Luis Obispo, California, USA

M. Blaskiewicz
Brookhaven National Laboratory, Upton, New York, USA

(Received 23 May 2024; accepted 23 December 2024; published 16 January 2025)

The electron-ion collider crab Cavities will present a significant transverse impedance to the beam. The low-level radio frequency system will have to reduce the crab cavity impedance to prevent transverse instabilities, while regulating the crabbing voltage and minimizing the radio frequency noise levels injected into the beam. This work presents an estimate of the crab cavity impedance in the presence of feedback and the resulting stability margins using simplified stability criteria. Generalized stability criteria are also presented in this work and are used to more accurately estimate stability margins.

DOI: 10.1103/PhysRevAccelBeams.28.011001

I. INTRODUCTION

The electron-ion collider (EIC) will provide unique capabilities for researchers to study quantum chromodynamics, the theory that describes how quarks and gluons interact to build protons, neutrons, and nuclei. The EIC will thus revolutionize the understanding of nucleon and nuclear structure and associated dynamics.

The EIC will reuse the Relativistic Heavy Ion Collider infrastructure [1]. The beams will collide with a 25 mrad full crossing angle. The EIC will employ crab cavities to compensate for the significant crossing angle, leading to an order of magnitude increase in luminosity [1]. The crab cavities will be used in a local scheme; crabbing and uncrabbing cavities will be paired around the sole interaction point. The crab cavity low-level radio frequency system (LLRF) will regulate the crabbing and uncrabbing voltages and try to maintain their sum to zero so that the crabbing is localized at the interaction region. The LLRF system will have to reduce the crab cavity impedance to prevent transverse instabilities. It will also have to maintain extremely low radio frequency (rf) noise levels injected to the beam.

Figure 1 shows a block diagram of the proposed crab cavity rf/LLRF. The rf feedback includes a narrowband integrator to regulate the mean value of the cavity voltage, as well as a proportional controller. This work studies the controller around individual stations, but, as the block diagram indicates, it might eventually be useful to add an additional controller that keeps the total crabbing and uncrabbing voltage to zero. Such a system would sample the cavity sum signal and act on one or all cavities. We refer to this system as the "global" controller. In addition, a one-turn feedback system (OTFB) is included for additional impedance control. The OTFB system has a high gain at the betatron sidebands of the revolution harmonics and a low gain at all other frequencies.

The LLRF objectives could lead to conflicting requirements. For example, a wider bandwidth would help transverse instability control but would significantly increase the noise injected to the beam. It is thus important to set the specifications for each of these items and then explore the trade-offs.

The transient beam loading effects have been studied [2]. These effects are expected to be very limited and should

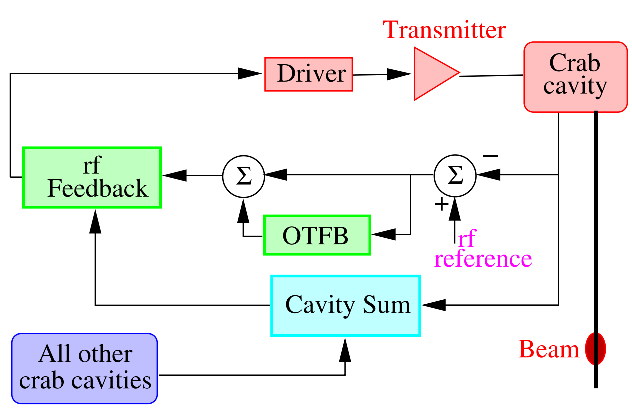

FIG. 1. Crab cavity rf/LLRF block diagram.

TABLE I. EIC parameters.

f_{rev} (kHz)	η	Q_s	σ_τ (ns)	I_0 (A)	E_T (GeV)
78.2	0.0019	0.010	0.2	1	275

only be considered for transmitter power specifications. The unclosed crab bump in the EIC will be in the order of 1.2 mm. This is comparable to the constant bunch position error of 0.6 mm used in [2]. Therefore, we also do not expect significant beam loading due to the unclosed crab bump.

The beam emittance growth due to rf noise studies is presented in [3]. rf noise is a significant challenge for the EIC, especially for the hadron storage ring (HSR). The LLRF design should prioritize minimizing rf noise injection. A dedicated feedback system to counteract rf noise effects has also been proposed and studied [4]. It could mitigate these effects and thus relax the crab cavity rf noise threshold. The performance of the system will greatly depend on its pickup precision, location, and additional technical specifications. The pickup is a critical component of this system, and the immediate future steps should be focused on its specifications.

This work studies the transverse instabilities due to the crab cavity impedance. Transverse instabilities are of much higher concern for the HSR rather than for the Electron Storage Ring. The higher beam energy requires higher β_x for a given voltage. We therefore present results for the HSR at 275 GeV. We also evaluate trade-offs with transient beam loading and rf noise reduction requirements.

Two sets of cavities will be used in the HSR: eight cavities operating at 197 MHz, and four cavities operating at 394 MHz. Table I presents critical EIC parameters used in this work, where f_{rev} is the revolution frequency, Q_s is the synchrotron tune, I_0 the DC beam current, E_T is the total particle energy, σ_τ is the rms bunch length (in time), and η is the frequency slip factor. The beam consists of 1160 bunches (evenly spaced every 10.2 ns), followed by a 1 μs long gap.

Table II presents crab cavity specific parameters. R_x is the transverse cavity resistance, f_r is the cavity fundamental frequency, τ_d is the loop delay, β_x is the beta function at the location of the impedance, and Q_L is the loaded quality factor. The EIC crab cavities will be on tune throughout the cycle.

The most critical time in the EIC cycle is right before collisions commence, since beam-beam effects are absent.

TABLE II. Crab cavity parameters.

f_r (MHz)	Q_L	$(R/Q)_t$ (Ω/m)	R_x (GΩ/m)	N_{cav}	τ_d (ns)	β_x (m)
197	1.75×10^6	2400	17.3	8	320	1300
394	1.75×10^6	1270	18.4	4	320	1300

Beam-beam effects increase the tune spread σ_ν and thus the stability margin. In this work, we use the tune spread before collisions, $\sigma_\nu = 14 \times 10^{-4}$.

The paper is organized as follows. Section II describes a modal domain description for the transverse impedance and the resulting growth rates and tune shifts. The most unstable modes for various LLRF configurations and *simplified* stability criteria and margins are presented in Sec. III. The *generalized* stability criteria used in this work are presented in Sec. IV, and the resulting stability margins are shown in Sec. V. Finally, we investigate trade-offs with the other LLRF requirements and alternative architectures in Sec. VI.

Transverse instabilities due to the crab cavity fundamental impedance are also of a concern for the High-Luminosity Large Hadron Collider (HL-LHC). Simulations have been performed to determine the required octopole current to achieve stability at the HL-LHC, with and without rf feedback and OTFB [5].

II. TRANSVERSE INSTABILITIES IN THE MODAL DOMAIN

As the beam passes through the crab cavities, a wake potential is formed [6]:

$$W_x(t) = H(t)\frac{R_x\omega_r}{Q_L}\sin(\omega_r t)e^{-\omega_r t/2Q_L}, \tag{1}$$

where $\omega_r = 2\pi f_r$ is the crab cavity fundamental angular frequency, t is the arrival time delay between the driving and kicked particle, and $H(t)$ is the Heaviside function. When comparing to [6], note that we use $t = -z/c$ as our variable to simplify imagining several bunches passing a fixed location over time. We note that for a leading particle with offset x_0, a particle trailing by a time delay τ gets the kick $c\Delta p_x = +q^2 x_0 W_x(\tau)$ as opposed to the negative sign in [6]. Physically, one checks that particles close to, but trailing, a leading particle are always pushed in the same direction at the offset of the leading particle. Application of the Panofsky-Wenzel theorem verifies that both the leading and closely trailing particles lose energy to the cavity.

To study these wakefields in the frequency domain, we define the transverse impedance according to [6]:

$$Z_x(\omega) = \frac{i}{\beta}\int_0^\infty e^{i\omega\tau}W_x(\tau)\,\mathrm{d}\tau, \tag{2}$$

where $\beta = v/c$. Here, our formulas are in exact agreement with [6].

Expanding the collective beam behavior in terms of revolution harmonics, the collective wakefield accumulation leads to a shift in the betatron oscillation of the beam, derived in [7]. For frequency shifts small compared to the synchrotron frequency, the complex betatron frequency shift for a Gaussian bunch can be approximated by [6]:

$$\Lambda_{m\mu} = -i\frac{ceI_0\Gamma(m+1/2)}{4\pi\omega_x E_T\sigma_\tau 2^{|m|}|m|!} \times \sum_n \frac{\beta_x}{\beta_x^{\text{smooth}}}\frac{Z_x(\omega_n)h_m(\omega_n-\omega_\xi)}{\sum_n h_m(\omega_n-\omega_\xi)}, \quad (3)$$

where m is the synchrotron mode, μ is the coupled-bunch mode, c is the speed of light, e is the charge of the electron, ω_x is the betatron angular frequency, $h_m(\omega)$ is the beam power spectral density (PSD) factor, ω_0 is the angular revolution frequency, ω_ξ is the angular frequency shift due to chromaticity, and the time evolution of the beam is $\propto \exp[-i(\omega_x+\Lambda_{m\mu})t]$.

The angular frequency shift due to chromaticity is given by $\omega_\xi = \omega_0\xi/\eta$, where $\xi = pdQ/dp$ is the unnormalized chromaticity. For this study, we used $\xi = +2$, leading to an angular frequency shift due to chromaticity of $\omega_\xi = 528$ mrad/s.

The ratio $\frac{\beta_x}{\beta_x^{\text{smooth}}}$ accounts for the local action of the impedance and is equal to 60.2 right before collisions and for the rest of the store. β_x^{smooth} is the average beta function in x from the smooth approximation [8].

We assume an even fill: the charge of the 1160 bunches is evenly distributed over 1260 equispaced buckets. This assumption is valid since the maximum growth rate for the partially filled ring is never more than the maximum growth rate for an evenly filled ring with the same total charge [9].

The impedance Z_x is evaluated at frequencies:

$$\omega_n = (nM+\mu)\omega_0 + \omega_x + m\omega_s, \quad (4)$$

where n is the rf mode, M is the number of equispaced bunches (1260), and ω_s is the synchrotron angular frequency. The growth rate is characteristic of the mode indexed by m and μ.

For a Gaussian bunch, the beam PSD factors are given by [6]

$$h_m(\omega) = (\omega\sigma_\tau)^{2m}e^{-\omega^2\sigma_\tau^2}.$$

Figure 2 shows $H_m(\omega-\omega_\xi) = h_m(\omega-\omega_\xi)/\sum_k h_m(\omega_k-\omega_\xi)$ for various values of m. Clearly, the modes of interest are the dipole ($m=0$) and head-tail ($m=1$).

It is important to note that the growth rate in Eq. (3) is proportional to both the beam current and the total transverse impedance sampled by the beam. Thus, uniformly lowering the impedance by a factor allows us to increase the beam current by the same factor, while maintaining the same complex betatron frequency shift. The imaginary part of this complex betatron frequency shift corresponds to the transverse growth rate, and the real part corresponds to the tune shift.

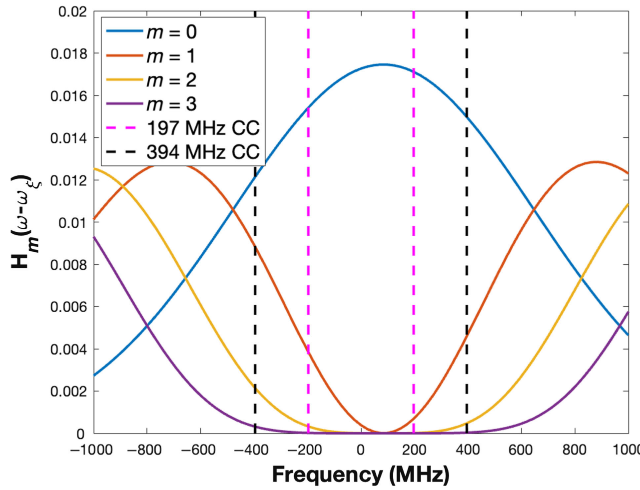

FIG. 2. Normalized weighting factors. Dashed lines represent the 197 and 394 MHz crab cavity fundamental frequency.

The crab cavity open-loop impedance as a function of frequency ω is given by [6]

$$Z_{x,ol}(\omega) = \frac{\omega_r R_x}{\omega[1+iQ_L(\omega_r/\omega-\omega/\omega_r)]}. \quad (5)$$

From Eq. (5), we can see that the impedance will peak at $\omega = \omega_r$. Thus, in the open-loop case, we expect a large complex betatron frequency shift near ω_r due to this resonance.

The rf feedback uses a probe to sample the crab cavity field, which depends on the crab cavity longitudinal impedance $Z_{||}(\omega)$ (circuits theory definition of impedance). $Z_{||}(\omega)$ is related to the transverse impedance:

$$Z_{||}(\omega) = \frac{\omega}{\omega_r R_x}Z_{x,ol}(\omega).$$

The feedback system then applies a correction to the transmitter input, proportional to this impedance, with a gain G_{fb}. The feedback loop includes a delay τ_d due to cables, waveguides, electronics, and the transmitter. The phase of the feedback loop path is adjusted to achieve a phase shift of zero at the cavity resonance. As a result, the feedback open-loop response is

$$H_{fb}(\omega) = G_{fb}e^{-i\Delta\omega\tau_d}Z_{||}(\omega),$$

where $\Delta\omega = \omega - \omega_r \text{sgn}\omega$ is the angular frequency offset from the crab cavity resonance. The closed-loop impedance in the presence of the rf feedback then becomes [10]

$$Z_{x,cl}(\omega) = \frac{Z_{x,ol}(\omega)}{1+H_{fb}(\omega)}. \quad (6)$$

The system performance is limited by the loop delay. The optimal gain is given by [11,12]

$$G_{\mathrm{opt}} = \frac{Q_L}{\omega_r \tau_d}.$$

For a delay of 320 ns, the resulting optimal gain is ≈4400 for the 197 MHz cavities and ≈2200 for the 394 MHz cavities. These gains lead to approximately 10 dB gain margin.

The OTFB is modeled according to [13] with a gain of 10. It provides an 11-fold decrease in the impedance at the betatron sidebands of each revolution harmonic. The OTFB filter response is given by

$$H_{\mathrm{OTFB}}(\Delta\omega) = G_c \frac{(1-\alpha_c)e^{\pm i2\pi(\nu_x \pm m\nu_s)} e^{-i(T_0-\tau_c)\Delta\omega}}{1-\alpha_c e^{\pm i2\pi(\nu_x \pm m\nu_s)} e^{-iT_0\Delta\omega}}, \quad (7)$$

where G_c is the OTFB gain, the parameter α_c controls the filter bandwidth around each betatron sideband, ν_x is the betatron tune, ν_s is the synchrotron tune, T_0 is the revolution period, and τ_c is the OTFB delay offset. Note that there are four notches between any two revolution harmonics, at $\pm\nu_x \pm m\nu_s$, for *each* nonzero m, and two notches at $\pm\nu_x$.

The parameters G_c and α_c are not independent [10]. To maintain rf loop stability with the same gain margin, the filter bandwidth is inversely proportional to the OTFB gain. As the gain is increased, the notch bandwidth eventually becomes comparable or smaller than the tune spread, thus reducing the effectiveness of the OTFB. Similarly, if there are significant tune shifts due to beam loading or imperfect settings, the OTFB notches might not be well aligned with the beam spectrum, further reducing its performance. These effects are included in the generalized Nyquist criteria (Sec. IV) but not in the simplified stability criterion (Sec. III). In this work, we use $\alpha_c = 15/16$, so that the OTFB bandwidth is approximately 780 Hz. For comparison, the tune spread in collisions is about 110 Hz.

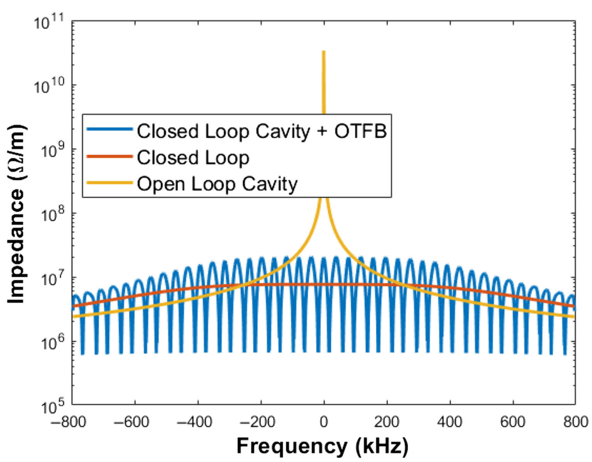

FIG. 3. Crab cavity transverse impedance magnitude ($m = 0$).

The open loop, closed loop, and closed-loop impedance with the OTFB ($m = 0$) are shown in Fig. 3.

The system's stability will be limited by the most unstable mode. The simplified stability criterion is proportional to the complex betatron frequency shift *magnitude* (for positive growth rates), with the proportionality constant determined by the transverse distribution [6]. As such, the magnitude of the most unstable betatron frequency shift is representative of the system stability. The most unstable modes are identified with this approach in Sec. III and then evaluated more accurately in Sec. V with the stability criterion presented in Sec. IV.

III. RESULTS OF MODAL DOMAIN MODEL

There are two significant contributions to the infinite sum in Eq. (3) around $\pm\omega_r$. Since the real part of the impedance is odd, but also symmetric around $\pm\omega_r$,

$$\mathbb{R}[Z_x(\omega_n)] = -\mathbb{R}[Z_x(-\omega_n)].$$

The growth rate—given by the imaginary part of the complex betatron frequency shift $\mathbb{I}(\Lambda)$—depends on the sum of these two impedances scaled by the PSD factor. Therefore the sign of the growth rate depends on

$$-[h_m(\omega_n - \omega_\xi) - h_m(-\omega_n - \omega_\xi)].$$

For $m = 0$, this is a negative number, and the corresponding modes are stable. For $m = 1$, this number is positive and the corresponding modes are unstable. In addition, due to the symmetry of both the impedance and the PSD factors, the growth rate is very small when the chromaticity is zero.

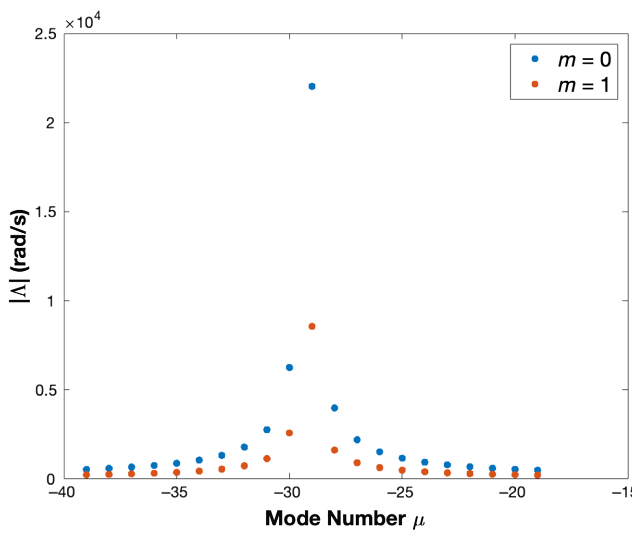

FIG. 4. Complex betatron frequency shift for $m = 0$ and $m = 1$ (open loop).

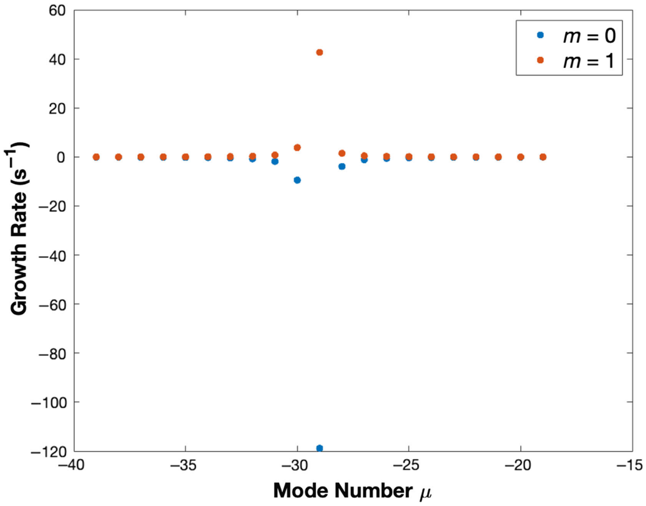

FIG. 5. Growth rates for $m = 0$ and $m = 1$ (open loop).

To test this conclusion, we used the modal domain model to study modes $m = 0$ and $m = 1$. Figures 4 and 5 show the resulting complex betatron frequency shift and growth rate for each mode in open loop. Not surprisingly, the most unstable mode is -29 (a betatron tune of 29.22 was used). Even though the complex betatron frequency shift is higher for $m = 0$, the growth rates are indeed all negative, therefore these modes are stable [6]. As a result, we focus on the $m = 1$ case.

We compare three cases for $m = 1$: the open-loop case, the closed-loop case with rf feedback, and the closed-loop case with rf and one-turn feedback [Eq. (7) with $m = 1$]. Figures 6 and 7 present the corresponding growth rates and tune shifts. In the open-loop case, the instability is dominated by the tune shift at mode -29. The rf feedback flattens and significantly lowers the impedance around the center frequency (Fig. 3), leading to much lower tune shifts.

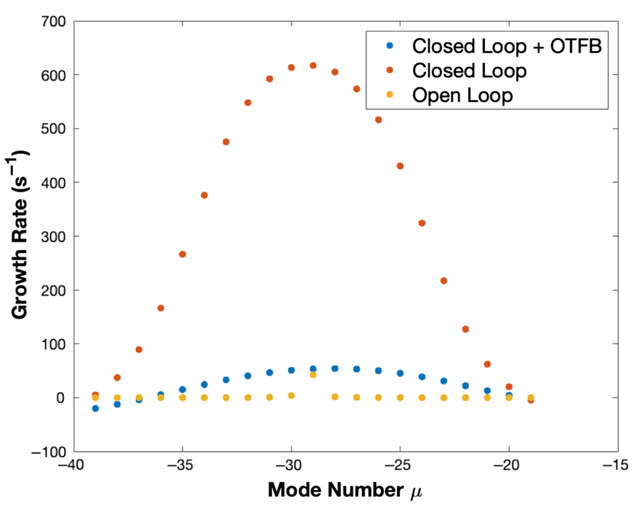

FIG. 6. Crab cavity transverse growth rates for different coupled-bunch modes with $m = 1$.

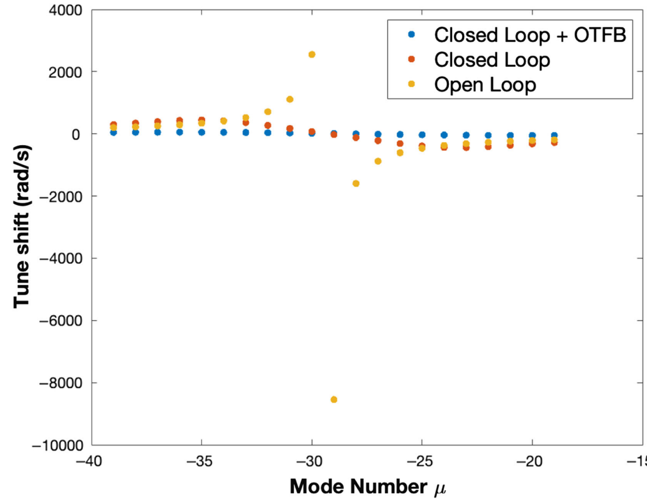

FIG. 7. Crab cavity transverse tune shift for different coupled-bunch modes with $m = 1$.

This results in a significant overall increase in stability for coupled-bunch modes around -29. The OTFB further reduces the impedance by roughly a factor of 11 and thus reduces the growth rate, tune shift, and complex betatron frequency shift.

Note that the growth rates are higher in closed loop than in open loop. The open-loop crab cavity bandwidth is very small (112 Hz for the 197 MHz cavities and 225 Hz for the 394 MHz cavities) compared to the offset of the closest betatron sideband ($\approx$17.2 kHz for a noninteger tune of 0.22 and f_{rev} of 78.2 kHz). As a result, the impedance sampled on the betatron sideband [Eqs. (3) and (4)] is mostly imaginary, leading to high tune shifts but low growth rates. The feedback action reduces and flattens the impedance, increasing the bandwidth by more than 3 orders of magnitude. As a result, even though the *magnitude* of the impedance is significantly reduced, the real part—and

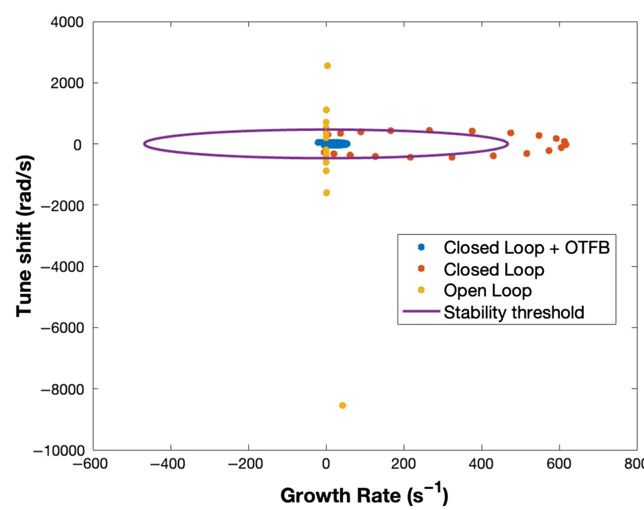

FIG. 8. Coupled-bunch stability margin.

TABLE III. Results of the modal domain model. The most unstable coupled-bunch mode (μ) and magnitude of betatron frequency shift are listed for each case.

Case	Mode	$\lvert\Lambda\rvert$ (s^{-1})
Open loop	−29	8545
Closed loop	−29	618
Closed loop + OTFB	−29	54.3

thus the growth rates—is increased for very low-order modes. This can also be seen in Fig. 8. The magnitude of the complex betatron frequency shift is significantly reduced in closed loop. The complex betatron frequency shift is close to the real axis (tune shift) in open loop, but close to the imaginary axis (growth rate) in closed loop.

Table III summarizes the most unstable mode and corresponding complex betatron frequency shift for each case. The stability margins for these cases are evaluated in Sec. V.

A. Simplified stability criteria

Simplified stability criteria can be used to *estimate* the stability margin for each of these cases. The advantage of the simplified criteria is that they can allow us to quickly evaluate various architectures and LLRF parameters. In addition, they help us visualize the frequency ranges of concern and appropriately adapt the LLRF. Once we narrow down the options, we can use the precise model presented in Sec. IV. It should be noted that this estimate does *not* include the effect of other transverse impedances or the beneficial effect of octupoles, since we use the tune spread without octupoles.

For coupled-bunch instabilities, we use the criterion presented in [6] for a normal distribution:

$$|\Lambda| < \frac{1}{\sqrt{3}}\Delta\omega_{1/2} = \sqrt{\frac{2\ln 2}{3}}\sigma_\nu\omega_0, \tag{8}$$

where $\Delta\omega_{1/2}$ is the tune distribution half width at half maximum. Figure 8 shows the resulting stability region, as well as Λ for the three cases of interest. The open-loop and closed-loop cases are unstable by a factor of $\approx$18 and $\approx$1.3, respectively. The closed loop with the OTFB has a stability margin of about $\approx$8.6.

The simplified stability criterion considers one mode at the time (3) and as such ignores mode coupling. Transverse mode coupling instabilities (TMCI) occur when the tune shifts of adjacent modes are comparable to the synchrotron tune ($Q_s = 0.010$ and thus $\omega_s = 4.9$ krad/s). Therefore, the simplified criterion for TMCI consists of checking the tune difference of adjacent modes as shown in Fig. 7. In open loop, the tune shift is significantly higher than the synchrotron tune, and thus the beam will be unstable. There are significant stability margins in closed loop and in the presence of the OTFB.

IV. TRANSVERSE INSTABILITIES IN THE FREQUENCY DOMAIN: GENERALIZED NYQUIST CRITERIA

The simplified criterion is very useful to quickly evaluate and compare different LLRF architectures and settings. Once the layout has been narrowed down though, a more precise calculation is required. This section presents the generalized stability criteria, which more accurately investigates the interaction between the beam dynamics and cavity impedance, including tune spread and tune shift.

For tune shifts that are comparable to the synchrotron tune, one must include coupling between the synchrotron modes. In addition, the Landau damping from octupoles or beam-beam effects is often important [14]. These effects can be included using a generalized Nyquist criteria [15]. Start by assuming a coupled-bunch mode with coherent frequency Ω. Let θ denote machine azimuth. The dipole moment of the beam is given by

$$\begin{aligned} D(\theta,t) &= I(\theta,t)\bar{x}(\theta,t) \\ &= \sum_{k=-\infty}^{\infty} D_k \exp[i(kM+\mu)(\theta-\omega_0 t) - i\Omega t)], \end{aligned} \tag{9}$$

where $\bar{x}(\theta,t)$ is the instantaneous centroid of the beam. Suppose the impedance is uniformly distributed so that the horizontal force per particle is given by

$$F_x(\theta,t) = \frac{q}{2\pi R}\int_0^\infty D(\theta,t-\tau)W_x(\tau)d\tau + \text{drive} \tag{10}$$

$$\begin{aligned} &= -i\frac{q}{2\pi R}\sum_{k=-\infty}^{\infty}[D_k Z_x(k) + d_k] \\ &\quad\times \exp[i(kM+\mu)(\theta-\omega_0 t) - i\Omega t)], \end{aligned} \tag{11}$$

where R is the radius of the accelerator, we have included an external drive and the impedance is evaluated at the revolution sidebands with

$$Z_x(k) = Z_x[(kM+\mu)\omega_0 + \Omega)]. \tag{12}$$

Instead of starting from the first principles, we will begin with a result from [16]. Assuming the betatron tune shift is small compared to the tune, we can use the single-sideband approximation. The coherent modes without Landau damping satisfy

$$D_n - \sum_{k=-\infty}^{\infty} T_{n,k} D_k = 0. \tag{13}$$

We start with equation 17-1 in [16] which was derived assuming uniform focusing. We make the substitution $v/\omega_x \to \beta_x$ to allow for the impact of localized impedances at large beta functions yielding

$$T_{n,k} = -i\frac{cqI_0}{4\pi RE_T}\sum_{m=-\infty}^{\infty} I_m(\tilde{n}\,\tilde{k}\,\sigma_\phi^2)\frac{1}{\Omega-\omega_x-m\omega_s} \times \sum_{\text{locations}} \beta_x Z_x(k) e^{-(\tilde{n}^2+\tilde{k}^2)\sigma_\phi^2/2}, \tag{14}$$

where $\tilde{n} = nM + \mu + Q_x - \xi/\eta$, $\tilde{k}$ is similar, $\sigma_\phi = \omega_r\sigma_\tau$, β_x is the beta function at the location of the impedance, and $I_m(x)$ is the modified Bessel function of the first kind of order m. This result is for a symmetric coupled-bunch mode, and we have used the betatron sideband appropriate to $\Omega \approx +\omega_x$. We also mention that our impedance definition in Eq. (2) differs by a minus sign from some other definitions [6,7], and we have allowed for multiple impedance locations.

With Eq. (14) as a starting point, we add Landau damping by substituting

$$\frac{1}{\Omega-\omega_x-m\omega_s} \to \tilde{I} \equiv -\int dJ_x dJ_y \frac{\partial F}{\partial J_x}\frac{J_x}{\Omega-\omega_x(J_x,J_y)-m\omega_s}. \tag{15}$$

In Eq. (15), $F(J_x, J_y)$ is the transverse action distribution that is normalized to unity. We assume that the details of the tune distribution have no significant impact and take:

$$\omega_x(J_x,J_y) = \omega_{x0} + \alpha_x J_x + \alpha_y J_y. \tag{16}$$

For the normalized transverse distribution, we take

$$F(J_x,J_y) = 6(J_{\max} - J_x - J_y)/J_{\max}^3 \quad \text{for } J_x + J_y < J_{\max}. \tag{17}$$

This allows the integral to be solved analytically, and we can choose the α's to get the right frequency spread. To present the results, we define

$$\hat{\Omega} + i\epsilon = \Omega - \omega_{x0} - m\omega_s, \qquad \hat{\alpha}_x = J_{\max}\alpha_x, \qquad \hat{\alpha}_y = J_{\max}\alpha_y.$$

Setting $x = J_x/J_{\max}$ and $y = J_y/J_{\max}$, Eq. (15) becomes

$$\tilde{I}(\hat{\Omega}+i\epsilon,\hat{\alpha}_x,\hat{\alpha}_y) = 6\int_0^1 x dx \int_0^{1-x}\frac{dy}{\hat{\Omega}+i\epsilon-\hat{\alpha}_x x - \hat{\alpha}_y y} \tag{18}$$

$$= \frac{3}{\hat{\alpha}_y}\left(\frac{\hat{\Omega}+i\epsilon-\hat{\alpha}_y}{\hat{\alpha}_x-\hat{\alpha}_y} - \frac{\hat{\Omega}+i\epsilon}{\hat{\alpha}_x}\right) + \frac{3}{\hat{\alpha}_y}\left(\frac{\hat{\Omega}+i\epsilon-\hat{\alpha}_y}{\hat{\alpha}_x-\hat{\alpha}_y}\right)^2\left(\frac{1}{2}\ln\left[\frac{\epsilon^2+(\hat{\Omega}-\hat{\alpha}_x)^2}{\epsilon^2+(\hat{\Omega}-\hat{\alpha}_y)^2}\right] - i\arctan\left[\frac{\hat{\Omega}-\hat{\alpha}_x}{\epsilon}\right] + i\arctan\left[\frac{\hat{\Omega}-\hat{\alpha}_y}{\epsilon}\right]\right)$$
$$-\frac{3}{\hat{\alpha}_y}\left(\frac{\hat{\Omega}+i\epsilon}{\hat{\alpha}_x}\right)^2\left(\frac{1}{2}\ln\left[\frac{\epsilon^2+(\hat{\Omega}-\hat{\alpha}_x)^2}{\epsilon^2+\hat{\Omega}^2}\right] - i\arctan\left[\frac{\hat{\Omega}-\hat{\alpha}_x}{\epsilon}\right] + i\arctan\left[\frac{\hat{\Omega}}{\epsilon}\right]\right). \tag{19}$$

Equation (16) is compared with results for a round Gaussian beam in Fig. 9. As is clear from the figure, it is possible to approximate a Gaussian fairly well, and Eq. (19) allows for roughly a 100-fold increase in speed over the numerical integrals needed for a Gaussian.

For stability analysis, we generalize Eq. (13) with modified matrix elements into a beam response problem:

$$D_n - \sum_{k=-\infty}^{\infty} T_{n,k}(\hat{\Omega}+i\epsilon)D_k = d_n, \tag{20}$$

where d_n is the amplitude of the drive at wavenumber n that includes the single particle response and ϵ is a small positive growth rate that ensures a causal response. Everything varies as $\exp[(\epsilon - i\hat{\Omega})t]$. We limit the sum to $N_- \le |k| \le N_+$, which is equivalent to band limiting the impedance, and view this as a matrix equation for vector $\mathbf{D}$:

$$[\mathbf{1} - \mathbf{T}(\hat{\Omega}+i\epsilon)]\mathbf{D} = \mathbf{d}. \tag{21}$$

For small current, $\mathbf{T} \to 0$ and the determinant of the matrix on the left goes to one. This is the key thing to notice. Consider a parametric plot of $\mathrm{Det}(\mathbf{1} - \mathbf{T}(\hat{\Omega}+i\epsilon))$ on the complex plane with parameter $\hat{\Omega}$. As the current is increased this contour will expand. At the stability threshold, the contour goes through 0. So, if this plot does not encircle 0, the beam is stable. To ensure stability in the $\epsilon \to 0$ limit, one varies ϵ in steps. By watching how the contours vary, it becomes clear if it is possible for the contour to encircle 0 at $\epsilon = 0^+$. One then takes a bunch

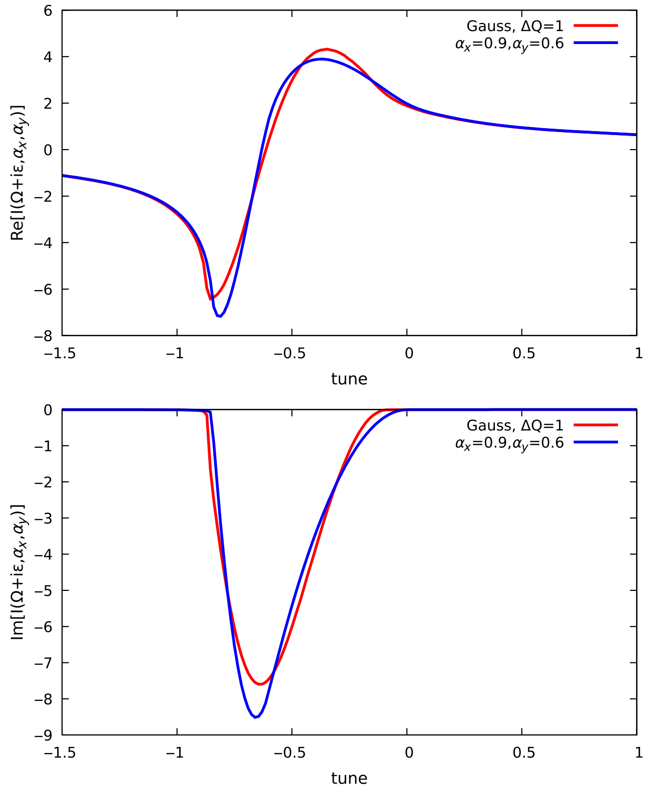

FIG. 9. Real and imaginary parts of Eq. (18) with $\hat{\alpha}_x = 0.9$ and $\hat{\alpha}_y = 0.6$ in comparison to a round Gaussian beam with a beam-beam parameter of 1. The frequency is in tune units with $\epsilon = 0.001$, and the tune shift for the Gaussian is taken from first-order perturbation theory. An offset in the tune axis has been added to improve alignment.

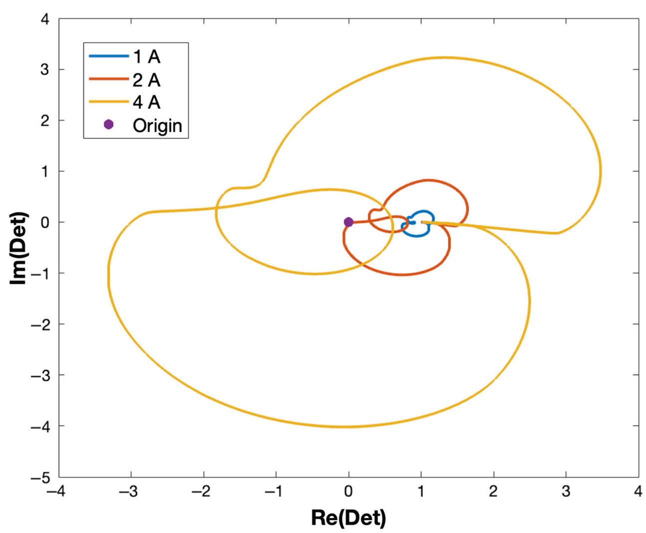

FIG. 10. Plot of $\mathbb{R}[\mathrm{Det}(\mathbf{1} - \mathbf{T}(\hat{\Omega} + i\epsilon))]$ vs $\mathbb{I}\{\mathrm{Det}[\mathbf{1} - \mathbf{T}(\hat{\Omega} + i\epsilon)]\}$ for $\mu = 29$ and for beam currents of 1, 2, and 4 A. The system is unstable when the contour encircles the origin.

charge that is sure to never have a contour that encircles 0. Strictly speaking, this is not an absolute threshold, but it is a safe value.

An example is shown in Fig. 10, which shows the closed-loop contour for beam currents of 1, 2, and 4 A. The threshold current is 2.1 A.

For scalar response functions, this is the well-known Nyquist stability criteria, and we call our technique the generalized Nyquist criteria [15]. Note that ϵ can be positive and large without breaking causality, so this technique can be used to calculate growth rates in unstable systems.

V. GENERALIZED NYQUIST CRITERIA RESULTS

The generalized Nyquist criteria (Sec. IV) can now be used to evaluate the most unstable coupled-bunch mode (μ) and determine the maximum dc beam current $I_{0,\max}$ for each case more accurately. These estimates are also compared to the simplified method for validation. The results are summarized in Table IV. The simplified and generalized criteria do lead to similar conclusions: the crab cavity impedance in open loop leads to instability. The closed-loop impedance is close to the stability threshold. The closed loop in the presence of the OTFB achieves a significant stability margin.

The simplified and generalized criteria have similar thresholds when the complex betatron frequency shift is dominated by the growth rate. The simplified criterion is more sensitive to increased tune shifts though, as seen in Fig. 5.5 in [6]. As a result, the two methods converge as the impedance is reduced. In open loop, the tune shift is orders of magnitude greater than the growth rate. The opposite is true in closed loop with the OTFB on. As a result, the simplified criterion provides reasonable estimates of the stability margin in the presence of feedback.

The current EIC technical specifications include a beam current of 1 A for the HSR at 275 GeV. From the table, we see that the open-loop system is unstable. The closed-loop system achieves stability, albeit with a narrow margin. The OTFB is required to achieve a significant operational margin. This study only considers the transverse impedance due to the two sets of crab cavities though, so the actual margin will be lower when other impedance sources are included.

TABLE IV. Results of generalized Nyquist criteria and comparison with the simplified stability criterion.

Case	Mode	Generalized $I_{0,\max}$ (A)	Simplified $I_{0,\max}$ (A)
Open loop	−29	0.4	Unstable
Closed loop	−29	2.1	0.75
Closed loop + OTFB	−28	8.5	8.6

VI. TRADE-OFFS WITH OTHER LLRF OBJECTIVES

As discussed in the introduction, the LLRF has to achieve three goals: to properly manage transient beam loading due to the induced voltage from the passing beam; to reduce rf noise in order to limit transverse emittance growth; and to reduce transverse impedance to prevent coupled-bunch instabilities. The first two of these goals are studied in [2] and [3]. A high LLRF gain/bandwidth is required to control the transverse instabilities. Such a setting significantly increases the crab cavity rf noise sampled by the beam. In this section, we explore trade-offs between impedance and noise reduction. In particular, we evaluate the effect of reducing the rf feedback gain (and thus reducing the bandwidth), of filtering the rf feedback response, and finally, of using different settings for the two sets of crab cavities (197 and 394 MHz).

A. Study of feedback gain

We might have to operate with lower rf feedback gain not only to reduce the LLRF bandwidth, but also because it might not be possible to get the dynamic range required for the optimal gain values (≈4400 and ≈2200 for the 197 and 394 MHz cavities, respectively, as shown in Sec. II). These values also correspond to a loop delay of 320 ns, which might prove hard to achieve.

We used the method presented in Sec. IV to evaluate the maximum stable beam current for different rf feedback gains G_{197} for the 197 MHz system. We present the maximum beam current $I_{0,\max}$ in the presence of only the 197 MHz system impedance (Z_{197}), as well as with the total impedance present ($Z_{197} + Z_{394}$). The OTFB is on for this study. The results are summarized in Table V. As expected, $I_{0,\max}$ evolves roughly linear with the gain when only the 197 MHz impedance is present, since the instability depends on the impedance at the fundamental that is decreased proportionally with the rf gain.

Introducing the 394 MHz impedance reduces the margin by about 50% for the nominal gain of 4400. As the 197 MHz gain is reduced, Z_{197} dominates, and the stability margin approaches the value without Z_{394}.

Reducing the rf feedback gain—and thus the rf bandwidth—by a factor of 2.5 reduces the stability margin roughly by a factor of 2. This might be a reasonable compromise given the *significant* associated reduction of rf noise sampled by the beam, as long as additional transverse impedance contributions do not *significantly* further reduce the stability margins.

TABLE V. $I_{0,\max}$ for different feedback gain values for the 197 MHz crab cavity LLRF.

$G_{197}/G_{\text{nominal}}$	0.4	0.8	1	1.2
$I_{0,\max}$ (A), Z_{197} only	6.7	12.9	16.2	19.5
$I_{0,\max}$ (A), $Z_{197} + Z_{394}$	4.8	7.6	8.5	9.3

Another approach would be to use different settings for the two crab cavity systems. Using the parameters from Table I, Eqs. (3)–(6), and the above gains, we can determine that the total contributions to the complex betatron frequency shifts from the two rf systems are comparable, with the 394 MHz system contributing about twice as much to the complex betatron frequency shift. The 197 MHz system has about double the $(R/Q)_t$ and twice as many cavities, but it can be operated with twice the gain and has approximately 3.5 times lower $h_m(\omega)$ values for $m = 1$. This relative contribution to growth rates is also evident in Table V.

On the other hand, the 197 MHz system is contributing *significantly* more to rf noise issues, due to the much higher voltage and the twice as many cavities. Thus, reducing the bandwidth of the 197 MHz system is far more critical. The 197 MHz system also has higher nominal gain, which might be hard to achieve.

As a result, a hybrid approach might be optimal: the 394 MHz system is operated at a nominal gain to reduce the impedance and contributions to transverse instabilities, whereas the 197 MHz system is operated at lower gain and bandwidth to significantly reduce rf noise effects with minimal effect on transverse instabilities. Therefore, the reduced G_{197} scenario explored in Table V might be desirable even if the ideal gain can be achieved.

B. Additional narrowband feedback loop

Another way to reduce the rf noise sampled by the beam is by carefully shaping the rf feedback response to achieve high gain around the fundamental (mode −29) while reducing the bandwidth. On the other hand, this approach

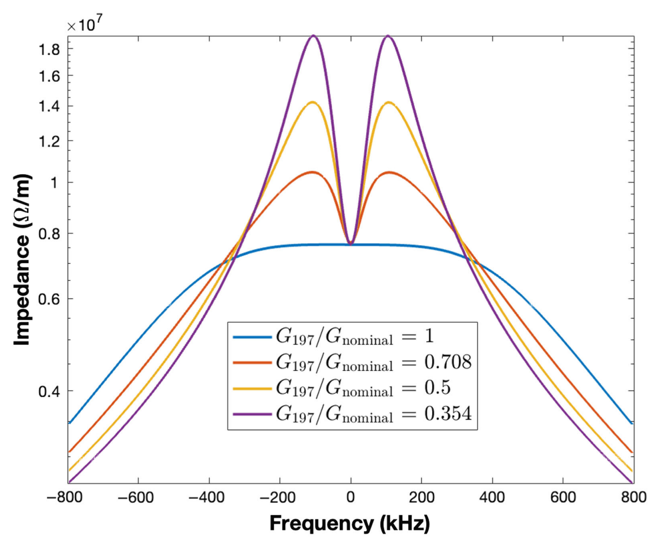

FIG. 11. Crab cavity transverse impedance magnitude ($m = 0$) as a function of G_{197}.

TABLE VI. $I_{0,\max}$ for various wideband and narrowband loop gains.

$G_{197}/G_{\mathrm{nominal}}$	1	0.707	0.5	0.354
Most unstable mode	−28	−27	−27	−27
$I_{0,\max}$ (A)	8.5	7.3	6.0	4.9

can increase the transverse instabilities for coupled-bunch modes away from the fundamental.

This could be achieved by reducing the gain of the proportional feedback, while adding a narrowband feedback loop with a bandwidth of ≈40 kHz, wide enough to cover the first betatron sideband. The narrowband loop gain is set to compensate for the reduced gain of the proportional controller and to thus achieve the same closed-loop impedance at the fundamental. Figure 11 shows the closed-loop impedance for various settings of the proportional controller gain for the 197 MHz cavities G_{197}.

Table VI presents the corresponding results. The ratio $G_{197}/G_{\mathrm{nominal}}$ is approximately equal to the closed-loop bandwidth reduction. Clearly, a significant reduction in bandwidth—and thus rf noise sampled by the beam—can be achieved with a modest reduction in the maximum beam current.

VII. CONCLUSIONS AND FUTURE STEPS

Transverse instabilities driven by the crab cavity fundamental impedance are of a concern for the EIC. In this work, we used a modal domain approach to identify the most unstable modes. These modes were then investigated in more detail using generalized Nyquist stability criteria. An LLRF architecture, including an rf feedback and an OTFB, leads to reasonable stability margins.

The optimal feedback gain leads to a wide LLRF bandwidth and thus results in a significant rf noise sampled by the beam and a high transverse emittance growth rate. Trade-offs between transverse instabilities and rf noise requirements were also presented in this work.

As the design matures, the tools developed for these studies will be valuable for future crab cavity LLRF investigations. The transverse stability limits will be updated once we establish the loop delay and evaluate the rf noise limits precisely.

ACKNOWLEDGMENTS

We want to thank P. Baudrenghien for his many contributions to this work through collaborations, conversations, and most importantly his studies of transverse instabilities due to the crab cavity fundamental impedance in the HL-LHC. This work is partially supported by the U.S. Department of Energy, Office of Science, Office of High Energy Physics, under Award No. DE-SC-0019287.

[1] F. Willeke and J. Beebe-Wang, Electron ion collider conceptual design report 2021, 2021, 10.2172/1765663.

[2] T. Mastoridis, K. Smith, T. Hidalgo, T. Loe, and M. Toivola, Time-domain simulation of the crab cavity/beam interaction, Brookhaven National Laboratory, Technical Notes No. BNL-224087-2023-TECH, 2023, 10.2172/1960268.

[3] K. Smith, T. Mastoridis, P. Fuller, P. Mahri, and Y. Matsumura, EIC transverse emittance growth due to crab cavity RF noise: Estimates and mitigation, Brookhaven National Laboratory, No. BNL-222748-2022-TECH, 2022, 10.2172/1846026.

[4] P. Baudrenghien and T. Mastoridis, Transverse emittance growth due to rf noise in crab cavities: Theory, measurements, cure, and high luminosity lhc estimates, Phys. Rev. Accel. Beams **27**, 051001 (2024).

[5] L. Giacomel, P. Baudrenghien, R. Calaga, X. Buffat, and N. Mounet, Mitigation strategies for the instabilities induced by the fundamental mode of the HL-LHC crab cavities, J. Instrum. **19**, P05046 (2024).

[6] A. Chao, *Physics of Collective Beam Instabilities in High Energy Accelerators*, Wiley Series in Beam Physics and Accelerator Technology (Wiley-Interscience, Hoboken, NJ, 1993).

[7] A. W. Chao, K. H. Mess, M. Tigner, and F. Zimmermann, *Handbook of Accelerator Physics and Engineering*, 2nd ed. (World Scientific, Singapore, 2013), 10.1142/8543.

[8] N. Mounet, The LHC transverse coupled-bunch instability, Ph.D. thesis, Ecole Polytechnique, Lausanne, 2012.

[9] R. D. Kohaupt, On multibunch instabilities for fractionally filled rings, DESY, Hamburg, Report No. DESY-85-139, 1985, https://cds.cern.ch/record/165205.

[10] P. Baudrenghien, Low level RF systems for synchrotrons: Part II: High intensity. Compensation of the beam induced effects, CERN, No. SL-Note-2001-028-HRF, 2005, 10.5170/CERN-2005-003.175.

[11] D. Boussard, Control of cavities with high beam loading, IEEE Trans. Nucl. Sci. **32**, 1852 (1985).

[12] P. Baudrenghien, G. Hagmann, J. Molendijk, R. Olsen, A. Rohlev, V. Rossi, D. Stellfeld, D. Valuch, and U. Wehrle, The LHC low level RF, Conf. Proc. C **060626**, 1471 (2006), https://accelconf.web.cern.ch/e06/PAPERS/TUPCH195.PDF.

[13] P. Baudrenghien, T. Mastoridis, and J. Molendijk, The LHC one-turn feedback, CERN Report No. CERN-ATS-Note-2012-025 PERF, 2012, https://cds.cern.ch/record/1424396.

[14] M. G. Minty *et al.*, Recent beam-beam experience with multiple high current bunches in PEP-II, in *Proceedings of the Workshop on Beam-Beam Effects in Large Hadron Colliders* (CERN, Geneva, Switzerland, 2000), pp. 20–27, https://inspirehep.net/literature/511170.

[15] M. Blaskiewicz, Landau damping with high frequency impedance, in *Proceedings of the 23rd Particle Accelerator Conference (PAC'09), Vancouver, BC, Canada* (JACoW, Geneva, Switzerland, 2021), pp. 4592–4594.

[16] J.-M. Wang, Modes of storage ring coherent instabilities, AIP Conf. Proc. **153**, 697 (1987).